Communications in Physics, Vol. 33, No. 2 (2023), pp. 195-204
DOI: https://doi.org/10.15625/0868-3166/17946

Characterization of structure and Li-ionic conductivity of $La_{2/3-x}Li_{3x}TiO_3$ ceramics prepared by spark plasma sintering

Le Dinh Trong†, **Nguyen Huu Tinh and Pham Van Hao**

Hanoi Pedagogical University 2, Phuc Yen, Vinh Phuc 280000, Vietnam

E-mail: †ledinhtrong@hpu2.edu.vn

Received 10 December 2022
Accepted for publication 29 December 2022
Published 23 April 2023

Abstract. *In this work, $La_{2/3-x}Li_{3x}TiO_3$ (LLTO) dense ceramic samples have been prepared by high-energy ball milling and spark plasma sintering (SPS) route. The crystal structures and microstructures of the samples were characterized by X-ray powder diffraction and FE-SEM, whereas their Li-ionic conductivity properties investigated by AC impedance spectroscopy. At 21°C, the LLTO ceramic samples possessed the grain conductivity and grain boundary/total conductivity of $\sigma_g = 8.3 \times 10^{-4}$ Scm^{-1} and $\sigma_{gb} = 2.3 \times 10^{-5}$ Scm^{-1}, respectively. In the investigated temperature range from 21°C to 120°C, the ion conduction is governed by thermally activated mechanism. The activation energies for grain and grain boundary conductivities are $E_{ag} = 0.26$ eV and $E_{agb} = 0.43$ eV, respectively.*

Keywords: high energy mechanical milling; LLTO ceramics; Spark plasma sintering; Lithium ionic conductivity; Impedance.

Classification numbers: 81.05.Je; 81.20.Ev; 72.20.-i; 61.72.Mm; 82.47.Aa; 84.37.+q.

1. Introduction

In recent years, lithium-ion batteries (LIBs) have been used as a popular power source for portable devices, hand tools, etc., due to their large specific capacity, long cycle life [1]. To expand the fields of using LIBs such as in high-temperature environments, in applications requiring large power such as electric cars, etc., researchers have been focusing on all-solid lithium-ion batteries (SLIBs), that use ceramic solid electrolytes. Batteries based on ceramic solid electrolytes are more suitable for applications involving high temperatures, they are structurally stable over

a wide temperature range, leak-proof, safer and have design flexibility [1, 2]. However, current solid electrolytes, that typically possess low ionic conductivity, cannot meet the required current density, especially for heavy-duty applications requiring high power [3, 4]. Therefore, the finding of inorganic solid electrolytes with high ionic conductivity, and good chemical stability in contact with the electrodes is very useful [5]. Among the promising inorganic solid electrolytes for SLIBs, perovskite-type lithium lanthanum titanium oxides $La_{2/3-x}Li_{3x}TiO_3$ (abbreviated as LLTO) have attracted considerable attention from researchers because of its high Li-ion conductivity, which can theoretically reach about 1×10^{-3} Scm^{-1}, at room temperature. However, according to the reported experimental results, the ionic grain conductivity of prepared LLTO can achieve about 10^{-3} Scm^{-1}, while the grain boundary conductivity is about two orders of magnitude lower than the grain conductivity (i.e. about 10^{-5} Scm^{-1}). Therefore, the total ionic conductivity for the polycrystalline LLTO samples is reduced to the order of 10^{-5} Scm^{-1} [6]. The research results also show that the lithium-ion conductivity of LLTO ceramics depends on the crystal structure and microstructure [6–8], the concentration of lithium-ion and the A-site vacancies [6, 7, 9, 10], the chemical homogeneity [5, 11], the sizes of grain and grain boundaries [12, 13] and material density [3]. The influence of these factors on the electrical conductivity of LLTO can be adjusted through the methods of initial LLTO powder preparation, temperature, time and sintering procedure [3, 5, 7, 14–18]. Therefore, preparation technology has always played an important role to obtain LLTO ceramics with desired properties.

To date, LLTO ceramics have mainly been synthesized by two methods, solid-state reaction [6, 8–10, 12, 14, 19–21] and sol-gel [7, 17, 18, 22] where the solid-state reaction method is often used that allows the production of a relatively large amount of materials. However, in order to obtain pure phases and compact pellets, this way usually requires a quite high-temperature (over 1300˚C) and a long-time processing [6, 8–10, 12, 14, 19–21] which can cause serious lithium loss even up to 20 mol% [14], wide particle size distribution, resulting in LLTO ceramics with less than expected conductivity. The sol-gel method allows the preparation of LLTO powders with uniform particle size, thereby improving the lithium ion conductive behaviors of LLTO ceramics, but the synthesis process is generally complicated and high cost due to the expensive input materials and in harmful influences to the environment.

In recent years, a high-energy ball mill method has been applied that allows LLTO powder to be obtained even at low temperature, with fairly uniform particle size, and to avoid loss of lithium when calcined at high temperature in a long time [15]. Furthermore, spark plasma sintering (SPS) is also used to prepare highly dense LLTO ceramics even at low temperature, in a short time [13, 23–25]. However, to be able to apply the SPS technique effectively when preparing LLTO ceramics, more detailed and systematic studies need to be continued.

In the present work, LLTO nano-powder was prepared by the high-energy ball milling technique. The as-prepared nano-powder was sintered by SPS technique for different isothermal hold durations. The microstructure, ionic conductivity properties were investigated in detail.

2. Experiment

$La_{2/3-x}Li_{3x}TiO_3$ nanopowder with $x = 0.09$ (LLTO) was prepared by mechanical alloying method using La_2O_3 (Aldrich - 99.9%), Li_2CO_3 (Aldrich - 99%) and TiO_2 (Aldrich - 99%) as source materials. The LLTO nanopowder preparation process using Fritsch model Pulverisette 6

high kinetic energy planetary mill has been reported in our previous work [15]. To obtain coin-shaped LLTO ceramic samples, the SPS system (LABOX-210, Sinter Land Corporation, Japan) was used. The LLTO powder was inserted into a 10 mm diameter graphite die and placed between the two electrodes. The samples were spark plasma sintered at a heating rate of 50°C min^{-1} from room temperature to 1050°C, which was kept at this temperature for 8 min, under a pressure of 60 MPa, in vacuum. The voltage and current of SPS were controlled according to the automatic operation mode. The samples were then cooled to near room temperature in the chamber that was air-filled to atmospheric pressure. After SPS, the samples were heat treated at 800°C for 3 h in air to promote re-oxidation. The LLTO ceramic density was determined by the well-known Archimedes method. The phase and crystalline structure of the prepared samples were determined by powder X-ray diffraction (XRD) using an EQUINOX 5000 diffractometer with CuK_α radiation ($\lambda = 1.54056$ Å), in the range of 2θ from 10° to 100° with a step of 0.015°. The microstructure of ceramic pellets was observed using a field-emission scanning electron microscope (FE-SEM) (S4800, Hitachi, Japan). For electrical measurement, 300 nm thick Au electrodes were prepared by vacuum deposition technique on two parallel surfaces of polished ceramic pellets. The ionic conductivity of the samples was determined by impedance spectrometry with the AutoLab PG-STAT302N instruments in combination with the FRA32M module, over the temperature range from 21 to 190°C and the frequency range from 0.1 to 106 Hz, in an atmospheric environment.

3. Results and discussion

Figure 1 shows the XRD patterns of LLTO powder after react-milling. From XRD patterns, it can be seen that beside the main LLTO phase, there is still a trace amount of residual titanium oxide rutile (TiO_2) after being milled for 6 h (Fig. 1a). The XRD pattern of the as-milled LLTO powder for 9 h shows only a single LLTO phase (Fig. 1b). The diffraction lines are not of great intensity, and widen, showing that the LLTO powder has been crystallized with a nanometer-sized grain size. The average grain size was estimated using the Scherrer equation

$$D = \frac{0.9 \times \lambda}{\beta . \cos\theta}, \tag{1}$$

where D is average grain size (nm), $\lambda = 0.154056$ nm (wavelength of X-ray sources), β is half-peak width (in radians), θ is Bragg's diffraction angle (in radians). Applying to diffraction lines corresponding to 2θ from 30° to 50°, the grain sizes of the as-milled LLTO powder for 6 h and 9 h were estimated to be 9.6 nm and 8.6 nm, respectively.

Figure 2 shows the typical XRD patterns of the LLTO ceramic samples after SPS. On the pattern of the sintered sample using the milled LLTO powder for 9 h, only diffraction peaks for a single phase of LLTO were detected (Fig. 2b). On the contrary, on the pattern of the sintered sample using milled LLTO powder for 6 h (Fig. 2a), some peaks appear at 2θ = 26.7° and 2θ = 20.3°, 35.6°, 52.6°, which are attributed to the impure phases of $La_4Ti_9O_{24}$ (according to PDF #36-0137) and $Li_2Ti_3O_7$ (according to PDF #35-0126), respectively. The failure to improve the purity of the source material could be due to the insufficiently high temperature and especially the short SPS time ($\leq$ 10 min) [24]. In addition to the obtained peaks from the base cell of cubic perovskite ABO3 (refer to PDF #46-0465), superstructure peaks (marked with arrows) are clearly observed. Further, no split of the (200) and (220) peaks was observed (insets in Fig. 2). Those show that the LLTO unit cell has tetragonal symmetry (space group P4/mmm; refer to PDF

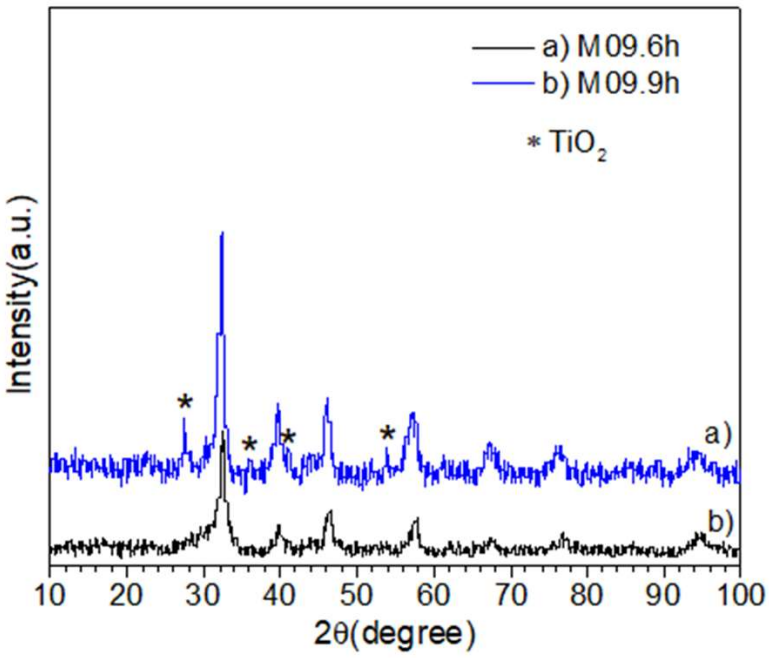

Fig. 1. XRD patterns of as-milled LLTO powder for 6 h (a) and 9 h (b).

#46-0466) [11, 12, 24]. The tetragonal cell is not simply a cube duplication along the c direction ($c \neq 2a$) as clearly indicated by the split of the (114) and (212) peaks (shown in the inset). The tetragonal distortion is attributed to the alternating distribution of La^{3+}, Li^+ cations and vacancies on the $a-b$ faces to La^{3+} rich (Li^+ and vacancy poor) and La^{3+} poor (Li^+ and vacancy rich) faces along c-axis [11, 19]. From XRD patterns in Fig. 2, the lattice parameters of LLTO ceramics were calculated being $a \approx 3.8795$ Å, $c \approx 7.7702$ Å, and $a \approx 3.8761$ Å, $c \approx 7.7534$ Å for the sintered sample using the ground LLTO powder for 6 h (M09.6 h) and that using grinded LLTO powder for 9 h (M09.9 h), respectively. In found, the lattice parameters of M09.6 h are slightly larger than those of M09.9 h. This is attributed to the fact that in the as-sintered M09.6 h there is still a small amount of $Li_2Ti_3O_7$ impurity, which reduces the lithium content in the LLTO phase, leading to an increase in its lattice parameters [17].

Figure 3 is the cross-sectional SEM micrographs of the SPS post-sintered samples. It can be seen that LLTO ceramic samples consist of quite uniform nano-sized grains. The direct grain-grain contacts dominate at the grain boundaries. The average grain sizes of samples, as roughly estimated from SEM micrographs of the sample's fractured surfaces, is about 780 nm. Using the Archimedes principle, the relative densities of the isothermal sintered LLTO pellets for 8 min was estimated to be around 90% of the theoretical X-ray density. According to Y. Kobayashi *et al.* [24], the relative density is only 76% as the SPS at 1000˚C. The density of LLTO ceramics can achieve over 95% of the theoretical X-ray density as the SPS at $\geq$ 1100˚C [24, 25], or under greater pressure [13].

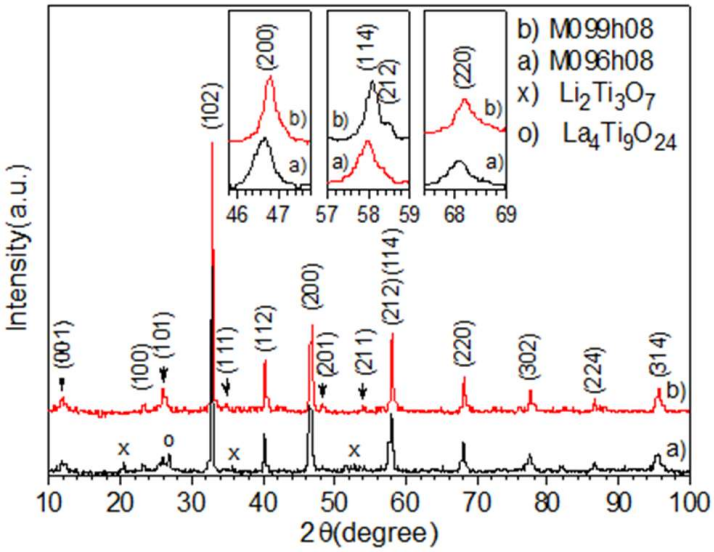

Fig. 2. Typical XRD patterns of as-sintered LLTO ceramics using milled LLTO powder for 6 h (a) and 9 h (b).

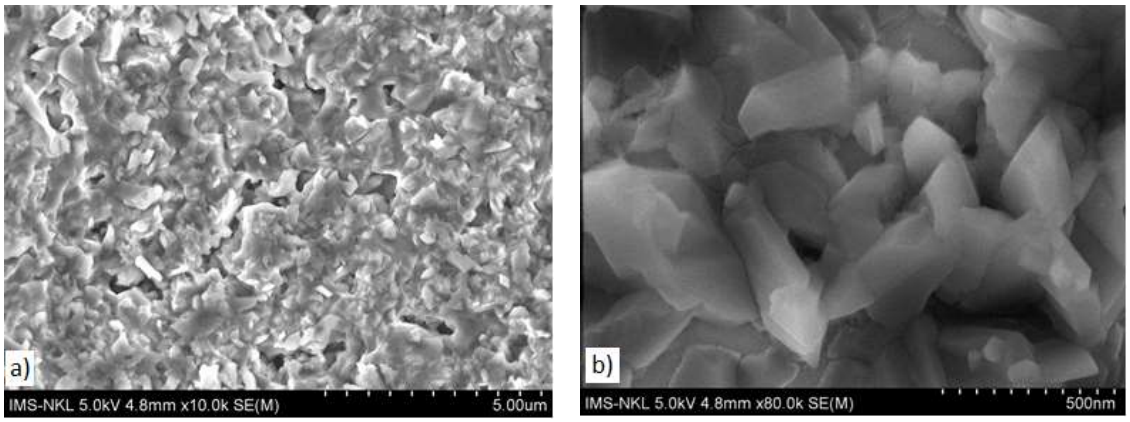

Fig. 3. Cross-sectional SEM micrographs of LLTO ceramic after SPS at 1050˚C for 8 min, with different magnifications.

In fact, Li-ionic conductivity of sintered samples using react-milled LLTO powder for 6 h was lower than that of sintered samples using react-milled LLTO powder for 9 h. The cause is attributed to the effect of the impure phases (especially $La_4Ti_9O_{24}$ which do not conduct lithium ions), although low in content, which are located within grain boundaries or inter-grains space, which cause inhibition of migration of Li^+ across the grain boundaries [24]. In addition, the existence of a $Li_2Ti_3O_7$ phase that reduces the carrier concentration, leading to a decrease in both grain and grain boundary conductivity [26]. In the following, the ionic conductive characteristics of the sintered samples using the react-milled powder for 9 h are presented only.

Figure 4 presents the typical impedance spectra (IS) recorded at room temperature (21˚C) of the ceramic samples. The impedance spectra consist of a semicircle in the high-frequency region related to grain and grain boundaries conductance. The intercepts of the semicircle with the Z'-axis towards the high frequency determine the grain resistance. The intercept of this semicircle with the Z'-axis towards the low frequency determine the total resistance which includes the contribution of the grain and the grain boundary components. The width of the semicircle determines grain boundary resistance. The second part is the straight line obtained in the low frequency region related to the diffusion process in the Helmholtz layer. To determine more precisely the ionic conductivity, the theoretical curve fitting method obtained from the equivalent circuit with the experimental data spectrum was used.

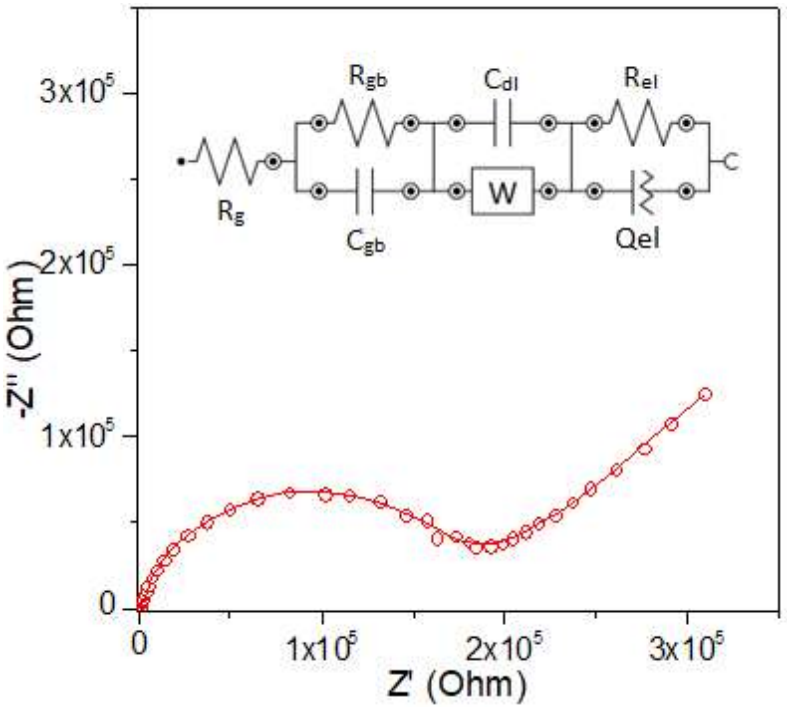

Fig. 4. Equivalent circuit and Cole–Cole plot for a typical complex impedance of LLTO of samples measured at room temperature (21˚C): the hollow circle represents experimental values; the solid line represents fitted data with an equivalent circuit.

Experimental IS data were recorded on samples with Au — LLTO — Au structure is well fitted with the plots obtained from the equivalent circuit shown by the inset in Fig. 4. Where, R_g is the resistance, which characterizes the grain conductance with capacitance C_g which can be neglected; R_{gb} and C_{gb} characterize the grain boundary conductance; W and C_{dl} - Warburg impedance characterizes the charge diffusion and capacitance of the Helmholtz layer at the electrode/LTTO interface; R_{el} and Q_{el}, resistance and constant phase element (CPE), respectively, which characterize the lithium ion blocking electrodes. The fitting results show that the C_{gb} capacitance is on the level of $\sim 10^{-9}$ F, in agreement with results reported by Wu *et al.* [13].

By fitting, the values of grain resistance (Rg) and grain boundary resistance (R_{gb}) were determined, the total resistance (R_T) is then $R_g + R_{gb}$. Using these resistances and sample dimensions, the conductivities are determined by the formula

$$\sigma = \frac{d}{R \times A}. \tag{2}$$

In formula (2), d is the thickness of the measured sample, A is the area of the Au electrode, and R is the measured real resistance (R_g, R_{gb} or R_T). The contributions of the Rg and R_{gb} to the R_T, the ionic conductivities of the SPS samples at room temperature (21˚C) are shown in Table 1. It shows that the contribution of R_{gb} to RT is predominant. Within error of 5%, the value of the total conductivity can be regarded as equal to that of the grain boundary conductivity. Therefore, the improved grain boundary conductivity will contribute mainly to the total conductivity improvement.

Table 1. Lithium ion conductivity of SPS samples at room temperature (21˚C).

Samples	R_g/R_T (%)	R_{gb}/R_T (%)	σ_g (Scm^{-1})	σ_{gb} (Scm^{-1})	σ_T (Scm^{-1})
M09.9h08	2.70	97.30	8.3×10^{-4}	2.3×10^{-5}	2.3×10^{-5}

The grain conductivity of SPS samples is consistent with that reported by Wu *et al.* [13]. Meanwhile, grain boundary conductivity is one order of magnitude larger than the reported results when the SPS process was carried out at the same 1050˚C for 3 min [24] and is consistent with that reported for the same composition prepared by conventional sintering at $\geq$ 1200˚C for 6-12 hours [7,12]. The high grain boundary conductivity (thus, the high total conductivity) is attributed to the high density of the prepared LLTO ceramics, and moreover, the improved grain - grain bonding at the atomic level in polycrystalline ceramics [25].

The temperature inverse dependence of $\ln(\sigma T)$ for the grain conductivity (σ_g) and grain boundary (σ_{gb}) of LLTO samples is shown in Fig. 5. In seen, the conductivity of the samples increased as increasing ambient temperature, un-following Arrhenius behavior in the entire investigated temperature range (294 – 463 K). In the temperature range higher than 400 K, a curvature of the $\ln(\sigma T)$ versus 1000/T plot is detected, which is especially evident for the grain conductivity. These results are consistent with the results of previously published works [20,21]. In the temperature range lower than 400 K, the plots of $\ln(\sigma T)$ versus 1000/T can be considered to follow the classical Arrhenius law:

$$\sigma = \frac{\sigma_0}{T} \exp\left\{-\frac{E_a}{kT}\right\}, \tag{3}$$

where σ_0 the pre-exponential factor, Ea - activation energy. The Li^+ conduction in this temperature range is of thermally activated mechanism.

From the temperature inverse dependence plots of $\ln(\sigma T)$, the activation energy for the ionic conductivity of the samples was determined. In temperature range lower than 400 K, the activation energy for the grain and grain boundary conductivities of the LLTO samples are 0.26 eV and 0.43 eV, respectively, consistent with the results reported by Wu *et al.* [13]. In the investigated temperature range higher than 400 K, the ionic conductivity of all samples did not obey Arrhenius law (2), the slope of the $\ln(\sigma T)$ versus $1000/T$ plots gradually decreased with increasing temperature. The non-Arrhenius behavior of ionic conductivity, at temperatures higher than

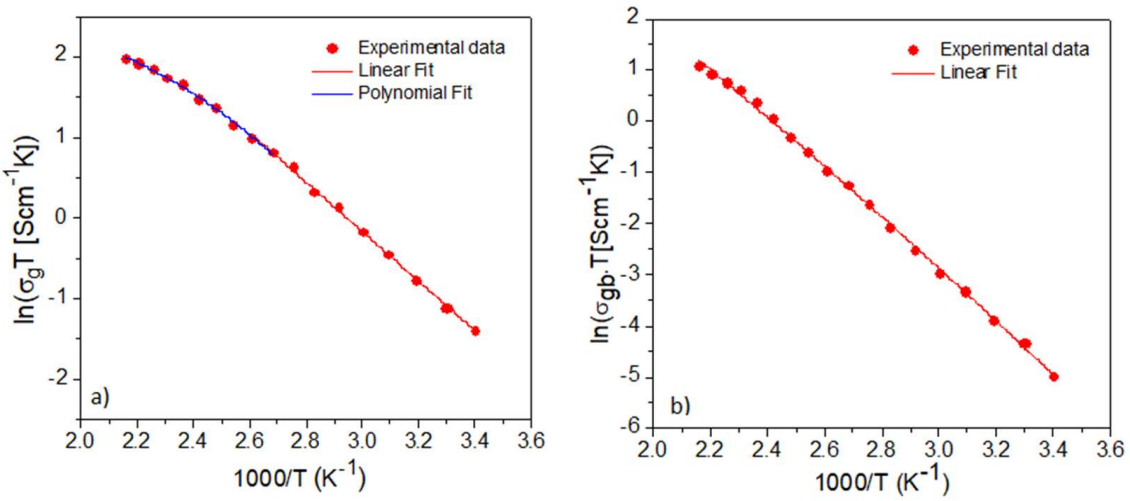

Fig. 5. Arrhenius plots of the grain (a) and grain boundary (b) conductivity for the ceramic specimens.

400 K, related to (i) the tilt or/and rotation of the TiO_6 octahedrons, leading to an "opening or closing of the bottleneck" in the perovskite through which lithium ions migrate into nearby A-site vacancies, and (ii) the relaxation of lattice, which becomes faster as the temperature increases and the ability of the lithium ions to jump backwards through the "bottleneck" decreases significantly, thus reducing activation energies [20].

4. Conclusions

This work confirmed that spark plasma sintering is an effective technique in preparing solid electrolyte of good ionic conductivity properties. The $La_{2/3-x}Li_{3x}TiO_3$ $(x = 0.09)$ pellets with fairly uniform grain size, relatively high density (over 90% of the theoretical X-ray density) were achieved by SPS technique at 1050°C, for a few minutes. The influence of LLTO precursor powder on the microstructure of LLTO ceramics was evaluated. At room temperature, the LLTO samples possessed grain conductivity of $\sigma_g = 8.3 \times 10^{-4}$ Scm^{-1}, and grain boundary conductivity of $\sigma_{gb} = 2.3 \times 10^{-5}$ Scm^{-1}. In the temperature region lower than 400 K, the temperature-dependent ionic conductivity obeys the Arrhenius law with the activation energies for the grain and grain boundary conductivities being $E_{ag} = 0.26$ eV and $E_{agb} = 0.43$ eV, respectively. Although the grain boundary conductivity has been improved, it is still nearly two orders of magnitude lower than the grain conductivity due to the low ceramic density and pores in the grain boundaries. In order to improve the total conductivity of LLTO ceramics, the optimization of the SPS process needs to be studied in more detail.

Acknowledgements

This work is supported by the Science & Technology Project (2019-2021) from Ministry of Education and Training (Project code: B2019-SP2-06)

Conflict of interest

The authors have no conflict of interest to declare.

References

[1] J. Janek and W. G. Zeier, *A solid future for battery development*, Nature Energy **1** (2016) 1.

[2] M.-M.Thackeray, C. Wolverton and E.-D. Isaacs, *Electrical energy storage for transportation-approaching the limits of, and going beyond, lithium-ion batteries*, Energy Environ. Sci. **5** (2012) 7854.

[3] R. Kali and A. Mukhopadhyay, *Spark plasma sintered/synthesized dense and nanostructured materials for solid-state Li-ion batteries: overview and perspective*, J. Power Sources **247** (2014) 920.

[4] A. Mauger, M. Armand, C. M. Julien and K. Zaghib, *Challenges and issues facing lithium metal for solid-state rechargeable batteries*, J. Power Sources **353** (2017) 333.

[5] G. Yang, C. Abraham, Y. Ma, M. Lee, E. Helfrick, D. Oh and D. Lee, *Advances in materials design for all-solid-state batteries: from bulk to thin films*, Appl. Sci. **10** (2020) 4727.

[6] J. Ibarra, A. Várez, C. León, J. Santamaría, L. M. Torres-Martínez and J. Sanz, *Influence of composition on the structure and conductivity of the fast ionic conductors* $La_{2/3-x}Li_{3x}TiO_3$ $(0.03 \leq x \leq 0.167)$, Solid State Ionics **134** (2000) 219.

[7] H. Geng, J. Lan, A. Mei, Y. Lin and C. W. Nan, *Effect of sintering temperature on microstructure and transport properties of* $Li_{3x}La_{2/3-x}TiO_3$ *with different lithium contents*, Electrochim. Acta **56** (2011) 3406.

[8] Y. Inaguma, T. Katsumata, M. Itoh, Y. Morii and T. Tsurui, *Structural investigations of migration pathways in lithium ion-conducting* $La_{2/3-x}Li_{3x}TiO_3$ *perovskites*, Solid State Ionics **177** (2006) 3037.

[9] K. Y. Yang, J. W. Wang and K. Z. Fung, *Roles of lithium ions and La/Li-site vacancies in sinterability and total ionic conduction properties of polycrystalline* $Li_{3x}La_{2/3-x}TiO_3$ *solid electrolytes* $(0.21 \leq 3x \leq 0.50)$, J. Alloys Compd. **458** (2008) 415.

[10] A. Dono and R. B. Cervera, *Solid state reaction synthesis and characterization of lithium lanthanum titanate lithium-ion conducting solid electrolyte with different Li to La content*, Key Eng. Mater. **821** (2019) 389.

[11] A. Mei, X.-L. Wang, J.-L. Lan, Y.-C. Feng, H.-X. Geng, Y.-H. Lin and C.-W. Nan, *Role of amorphous boundary layer in enhancing ionic conductivity of lithium–lanthanum–titanate electrolyte*, Electrochim. Acta **55** (2010) 2958.

[12] A. C. Sutorik, M. D. Green, C. Cooper, J. Wolfenstine and G. Gilde, *The comparative influences of structural ordering, grain size, Li-content, and bulk density on the* Li^+*-conductivity of* $Li_{0.29}La_{0.57}TiO_3$, J. Mater. Sci. **47** (2012) 6992.

[13] J. F. Wu and X. Guo, Size effect in nanocrystalline lithium-ion conducting perovskite: $Li_{0.30}La_{0.57}TiO_3$, Solid State Ionics **310** (201) 38.

[14] C. W. Ban and G. M. Choi, *The effect of sintering on the grain boundary conductivity of lithium lanthanum titanates*, Solid State Ionics **140** (2001) 285.

[15] L. D. Trong, N. N. Dinh and P. D. Long, *Annealing effect on the ionic conductivity of* $La_{0.67-x}Li_{3x}TiO_3$ *made by double mechanical alloying method*, J. Mater. Sci. Eng. B **4** (2014) 86.

[16] T. Zinkevich, B. Schwarz, P. Braun, A. Weber and H. Ehrenberg, *Effect of sintering temperature on Li diffusivity in Li0.29La0.57TiO3: local hopping and long-range transport*, Solid State Ionics **357** (2020) 115486.

[17] H. Geng, A. Mei, Y. Lin and C. W. Nan, *Effect of sintering atmosphere on ionic conduction and structure of* $Li_{0.5}La_{0.5}TiO_3$ *solid electrolytes*, Mater. Sci. Eng. B **164** (2009) 91.

[18] G. B. Kunshina, O. B. Shcherbina and V. I. Ivanenko, *Study of transport properties and microstructure of lithium-conducting Li0.33La0.56TiO3 ceramic*, Russ. J. Appl. Chem. **92** (2019) 1351.

[19] J. L. Fourquet, H. Duroy and M. P. Crosnier-Lopez, *Structural and microstructural studies of the series* $La_{2/3-x}Li_{3x}\square_{1/3-2x}TiO_3$, J. Solid State Chem. **127** (1996) 283.

[20] O. Bohnke, C. Bohnke anf J. L. Fourquet, *Mechanism of ionic conduction and electrochemical intercalation of lithium into the perovskite lanthanum lithium titanate*, Solid State Ionics **91** (1996) 21.

[21] O. Bohnke, J. Emery and J. L. Fourquet, *Anomalies in* Li^+ *ion dynamics observed by impedance spectroscopy and 7Li NMR in the perovskite fast ion conductor* $(Li_{3x}La_{2/3-x}\square_{1/3-2x})TiO_3$, Solid State Ionics **158** (2003) 119.

[22] I. C. Popovici, E. Chirila, V. Popescu, V. Ciupina, G. Prodan, *Sol–gel preparation and characterization of perovskite lanthanum lithium titanate*, J. Mater Sci. **42** (2007) 3373.

[23] Y. Kobayashi, H. Miyashiro, T. Takeuchi, H. Shigemura, N. Balakrishnan, M. Tabuchi M., H. Kageyama, T. Iwahori, *All-solid-state lithium secondary battery ceramic/polymer composite electrolyte*, Solid State Ionics **152–153** (2002) 137.

[24] A. Mei, Q. H. Jiang, Y. H. Lin and C. W. Nan, *Lithium lanthanum titanium oxide solid-state electrolyte by spark plasma sintering*, J. Alloys Compd. **486** (2009) 871.

[25] Y. Leyet, F. Guerrero, J. Anglada-Rivera, I. Martinez, H. Amorin, Y. Romaguera-Barcelay *et al.*, *Obtention of $Li_{3x}La_{2/3-x}TiO_3$ ceramics from amorphous nanopowders by spark plasma sintering*, Ferroelectrics **498** (2016) 62.

[26] J. S. Pereira, F. Guerrero, Y. Romaguera-Barcelay, J. Anglada-Rivera, J. C. C. Sales Jr, R. S. Silva *et al.*, *$La_{0.59}Li_{0.24}TiO_3$ ceramics obtained by spark plasma sintering: electric behavior analysis*, Mater. Res. Express **6** (2019) 1.